

This journal is © The Royal Society of Chemistry 2016

**Electronic Supplementary Information (ESI) for:
Local electronic properties of individual Pt atoms
adsorbed on TiO₂(110) studied with Kelvin probe
force microscopy and first-principles simulations**

Ayhan Yurtsever,^{*,†,‡,¶} Delia Fernández-Torre,^{§,||} Jo Onoda,^{†,⊥} Masayuki Abe,[¶]
Seizo Morita,^{†,‡} Yoshiaki Sugimoto,^{†,⊥} and Rubén Pérez^{*,§,#}

E-mail: ayhan@afm.eei.eng.osaka-u.ac.jp; ruben.perez@uam.es

*To whom correspondence should be addressed

[†]Graduate School of Engineering, Osaka University, 2-1 Yamada Oka, Suita, Osaka, 565-0871, Japan

[‡]The Institute of Scientific and Industrial Research, Osaka University, 8-1 Mihogaoka, Ibaraki, Osaka 567-0047, Japan

[¶]Graduate School of Engineering Science, Osaka University, 1-3 Machikaneyama, Toyonaka, Osaka 560-8531, Japan

[§]Departamento de Física Teórica de la Materia Condensada, Universidad Autónoma de Madrid, E-28049 Madrid, Spain

^{||}Instituto de Estructura de la Materia, CSIC, Serrano 121, 28006 Madrid, Spain

[⊥]Department of Advanced Materials Science, Graduate School of Frontier Sciences, University of Tokyo, 5-1-5, Kashiwanoha, Kashiwa, Chiba 277-8561, Japan

[#]Condensed Matter Physics Center (IFIMAC), Universidad Autónoma de Madrid, E-28049 Madrid, Spain

ADDITIONAL EXPERIMENTAL DATA

Constant–height LCPD maps

In order to prevent the topographic crosstalk in KPFM maps due to tip motion across a surface corrugation, we used retrace scanning at a constant-height to register an image of the LCPD map above the h -TiO₂(110) surface. However, we did not find significant differences between these two modes. Fig. S1(a) and (b) show the NC-AFM frequency shift (Δf) and simultaneously obtained KPFM images of the h -TiO₂(110) surface, acquired at constant-height using a neutral (upper part) and a protrusion mode tip (lower part), respectively. The KPFM images show the same basic features as observed in Fig. 1(b) and (f) of the main manuscript. The effect of constant-height KPFM measurements on the LCPD contrast formation is demonstrated in Fig. S2 using the same tip-apex termination. Fig. S2(a) and (b) show the NC-AFM topography and the corresponding KPFM images of the h -TiO₂(110) surface acquired with a neutral mode tip. The constant-height KPFM image of the same surface region is shown in Fig. S2(d), which was acquired using the same tip-apex as used in Fig. S2(a) and (b). As can be seen in Fig. S2(b) and (d), the LCPD maps show identical contrast over OH atomic sites. The histogram analysis of the acquired LCPD data over the scanned area shown in Fig. S2(b) and S2(d) reveals two distinct peaks, which can be attributed to the H atoms (lower potential) and the bare TiO₂(110) surface (higher potential) (see Fig. S2(e)).

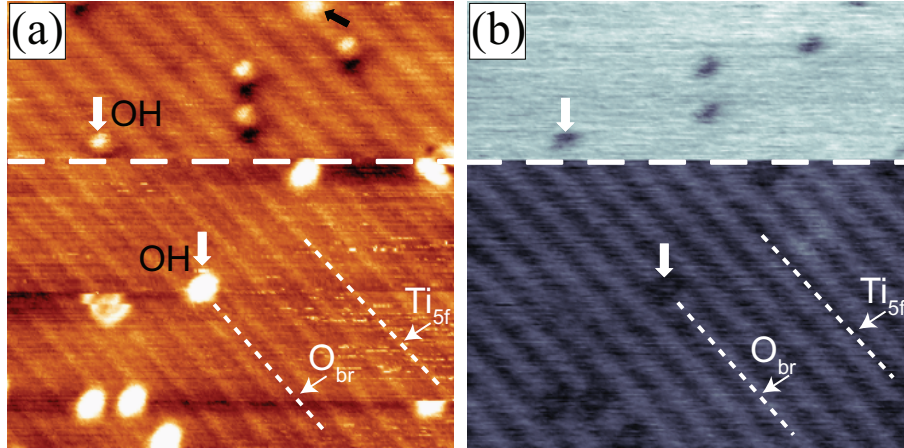


Fig. S1: (a) ($10 \times 10 \text{ nm}^2$) Frequency shift (Δf) and (b) simultaneously obtained KPFM images of the hydroxylated $\text{TiO}_2(110)$ surface, obtained using retrace scanning at a constant-height. While the upper part is recorded with a neutral mode tip, the lower part of the image is acquired with a protrusion mode tip. The contrast above H atoms in the LCPD maps for both imaging modes is shifted to lower LCPD values compared to the substrate, and the contrast above O_{br} atomic rows displays a higher LCPD with respect to the Ti_{5f} atomic rows. The atomic feature highlighted by a black arrow in (a) can be attributed to a residual impurity located on Ti_{5f} and/or in-plane oxygen vacancy site. Acquisition parameters: $f_0 = 159.543 \text{ kHz}$, $A = 14.3 \text{ nm}$. KPFM parameters: $U_{ac} = 0.5 \text{ V}$, $f_{ac} = 500 \text{ Hz}$.

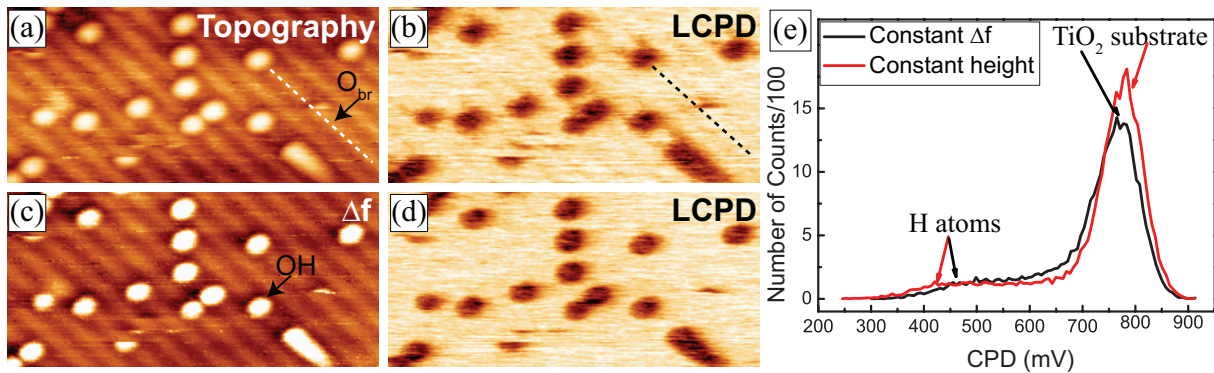


Fig. S2: (a) ($10 \times 4.75 \text{ nm}^2$) NC-AFM topography and (b) simultaneously obtained KPFM images of the hydroxylated $\text{TiO}_2(110)$ surface, acquired with a neutral mode tip at room temperature. (c) Δf and (d) simultaneously recorded KPFM images of the same surface region shown in (a), obtained using retrace scanning at a constant-height. (e) Histogram of the LCPD map acquired over the KPFM image in (b) and (d), showing two different distributions of LCPD values, which can be attributed to the H atoms and bare TiO_2 substrate, as labeled accordingly. The LCPD contrast difference between the H atoms and TiO_2 substrate is about $\sim 350 \text{ meV}$. Note that the LCPD contrast difference between H and TiO_2 substrate is almost identical for these two different measurements modes. Acquisition parameters: $f_0 = 155.531 \text{ kHz}$, $A = 13.0 \text{ nm}$, $\Delta f = -4.6 \text{ Hz}$. KPFM parameters: $U_{ac} = 0.5 \text{ V}$, $f_{ac} = 500 \text{ Hz}$.

Reliability of the distance-dependent LCPD spectroscopy measurements

In this supporting information, we provide additional experimental data sets to support the reliability of the local contact potential difference (LCPD) measurements of individual Pt atoms adsorbed on h -TiO₂(110) surface. The data presented here were acquired with a different cantilever than the one used to obtain the results of Fig. 3(a) and (b) in the main manuscript. In order to determine the tip-sample interaction regimes, we also include the calculated short-range interaction forces for both protrusion and hole mode tips. It should be noted that these calculated short-range interaction forces have been reported in our previous study.¹

Fig. S3(a) shows the total frequency shift-distance ($\Delta f-z$) curves acquired over Pt (green line), O_{br} atom (red line), Ti_{5f} (blue line), and OH group (black line), which were acquired with a tip producing protrusion mode image contrast of the surface. It needs to be mentioned that the site-specific $\Delta f-z$ curves were acquired with KPFM compensation in active condition. Fig. S3(b) shows the variation of the V_{LCPD} as a function of tip-sample separation obtained using an active KPFM feedback to nullify existing electrostatic forces at each particular distance. We observe a decrease in the LCPD of Pt and OH group which can be distinguished from the underlying substrate. As seen in Fig. S3(b), the LCPD of Pt deviates from the substrate LCPD (i.e., the LCPD over O_{br} and Ti_{5f} atomic rows) around $z \leq 6$ Å, and that of H atom deviates around $z \leq 5$ Å, which are in good agreement with the theoretically obtained results (see Fig. S3(d) for comparison). On the contrary, the LCPD over the surface O_{br} and Ti_{5f} atomic rows does not deviate from a constant value almost over the complete tip-sample distance range. One of the most striking features in Fig. S3(b) is the characteristic distance dependence of LCPD on Pt over a distance range between 4.8 and 6 Å away from the surface. The LCPD at this distance regime exhibits a weak distance dependence, showing an identical behavior as the LCPD curve shown in main manuscript (see Fig. 3(b)). We attribute this characteristic behavior of LCPD acquired over Pt atom to the presence of intrinsic dipole resulting from the Pt-TiO₂(110) charge transfer, pointing towards the vacuum.

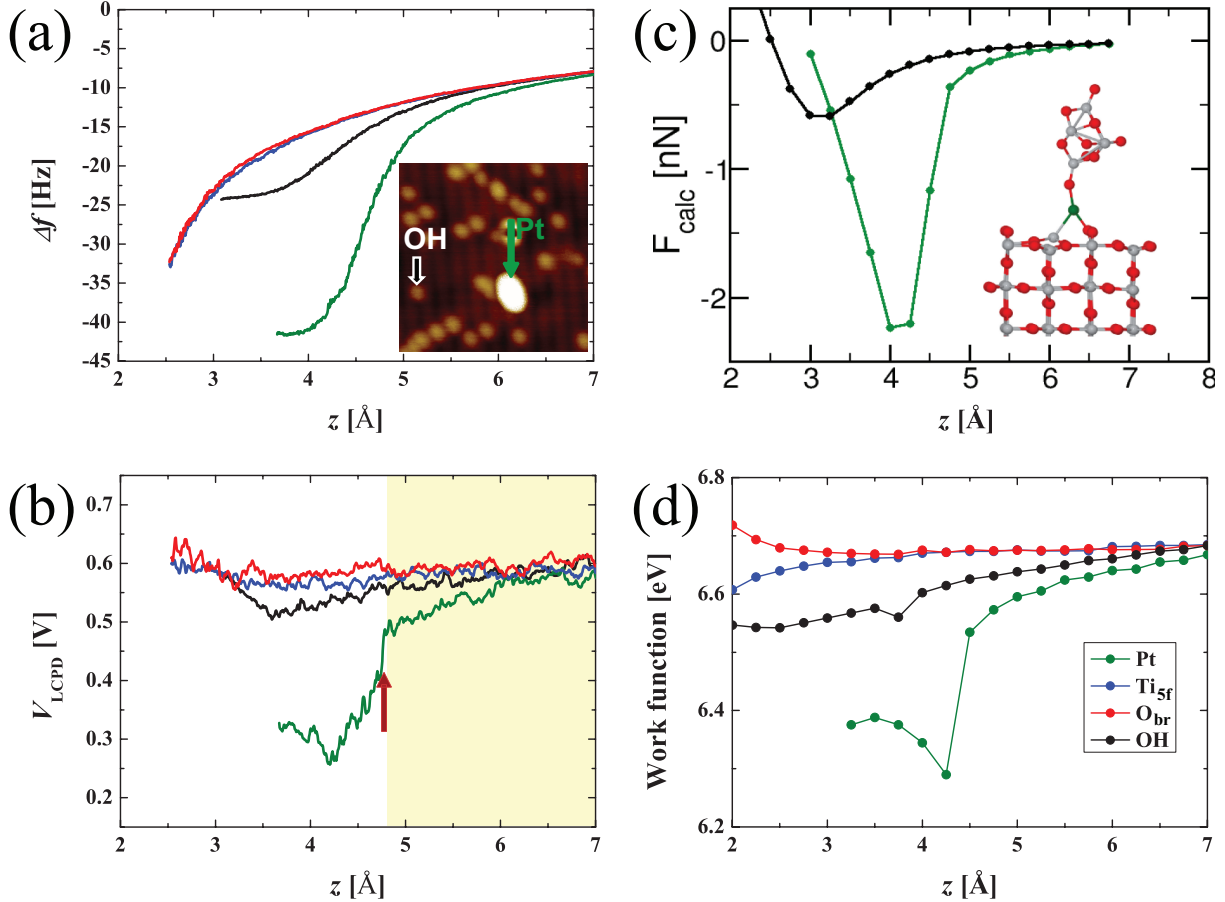


Fig. S3: (a) The averaged total frequency shift-distance (Δf - z) curves acquired over Pt (green line), O_{br} atom (red line), Ti_{5f} atom (blue line), and OH group (black line), which were obtained with a tip generating protrusion mode contrast. Inset: (7.5×7.5 nm²) NC-AFM image showing the individual Pt atom over which the spectroscopic measurements were performed. (b) Variation of the V_{LCPD} as a function of tip-sample separation obtained using an active KPFM feedback. (c) Calculated short-range force vs distance curve over the Pt and OH atomic sites. Inset: tip-sample structure over the Pt site at $z = 4.25$ Å. (d) Calculated variation of the local work function upon approaching the protrusion-model tip over Pt, O_{br} , Ti_{5f} , and OH sites. Since the absolute z values are unknown, the z -axis of the experimental curves has been shifted to adjust the position of the attractive force maximum of the Pt atom to the theoretical curves. Acquisition parameters: $f_0 = 166.4259$ kHz, $A = 6.45$ nm, $\Delta f = -14.4$ Hz. KPFM parameters: $U_{ac} = 0.2$ V, $f_{ac} = 500$ Hz.

It should be emphasized that the calculated short-range interaction force (F_{SR}) over Pt and OH site can be used to estimate the tip-sample distances (see Fig. S3(c)). The distance reference has been determined by aligning the attractive force maxima on the Pt atom with the theoretically calculated results (Fig. S3(c)). Fig. S3(d) shows the calculated variation of the local work function upon approaching the protrusion model tip over the Pt, OH, O_{br} , and Ti_{5f} sites. The similarity between the data presented in Fig. S3(b) and the one in Fig. 3(b) of the main manuscript is clearly evident. The tip-sample distances associated LCPD changes very much resemble those in Fig. 3(b) of the main manuscript. Similar results have been repeatedly observed for different experiments: we thus conclude that the LCPD curves obtained by the tips producing protrusion mode contrast are reproducible.

In Fig. S4(a), we show the calculated F_{SR} over Pt and O_{br} atoms for the hole mode tip to determine the interaction regions. It is worth nothing that the nature of the tip-sample interaction and the contrast mechanisms for the case of hole mode tip can be found in ref.¹ The work function change obtained with a hole imaging mode tip displays the same constant value for both Pt and O_{br} sites up to 3.5 Å, and raises when the tip enter the repulsive branch of the interaction force and separated from the background surface work function (see Fig. S4(b)). However, we were not able to collect KPFM images in that distance range. Therefore, the hole mode tip is not so useful for the measurements of LCPD changes induced by individual adsorbates on the *h*-TiO₂(110) surface.

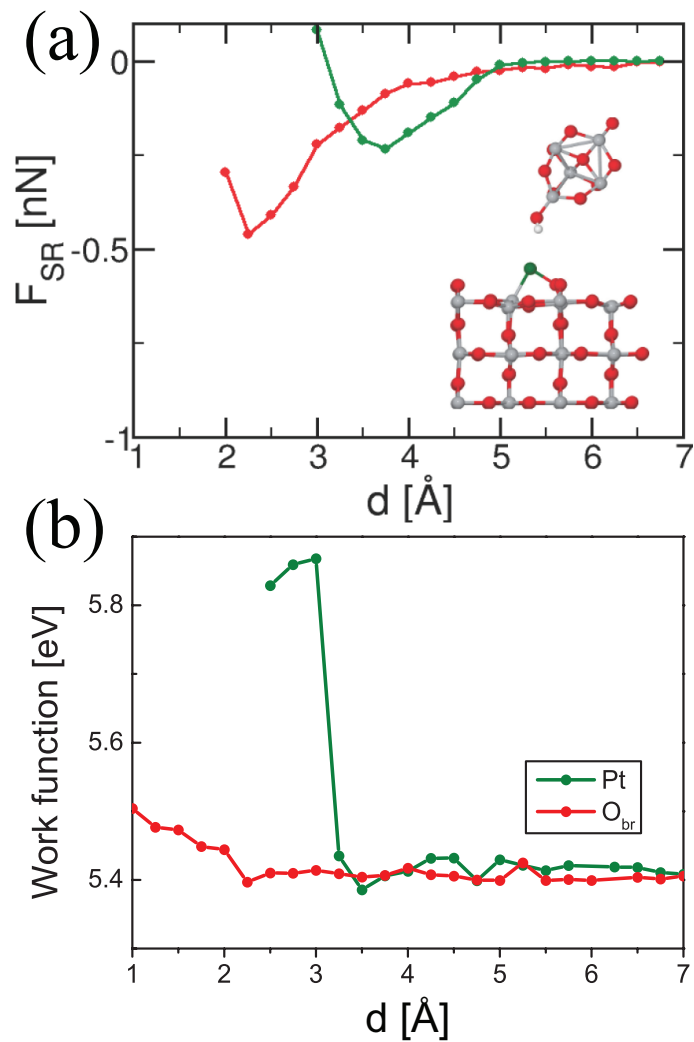


Fig. S4: (a) Calculated short-range force (F_{SR}) over Pt (green line) and O_{br} (red line) for the hole mode tip. Inset: tip-sample structure over the Pt site at $d = 3.0$ Å. (b) Calculated variation of the local work function upon approaching the OH-terminated TiO_2 -based cluster tip above the Pt and O_{br} atomic sites.

Charge transfer analysis between model tip and Pt/TiO₂

Bader charge analysis has been performed to investigate the charge transfer between a protrusion model tip and Pt/TiO₂ surface as a function of tip-sample distance (z). We found that an electron transfer between our model tip and Pt (OH) occurs at $z < 5.5$ Å ($z < 4.5$ Å) (Fig. S5). The occurrence of such charge transfer is also confirmed by the analysis of the projected density of states (PDOS), which show that the tip-induced electronic states fall above the Pt/TiO₂ Fermi level, thus indicating that the tip donates charge to Pt and OH atomic sites below a certain tip-sample distance (not shown here).

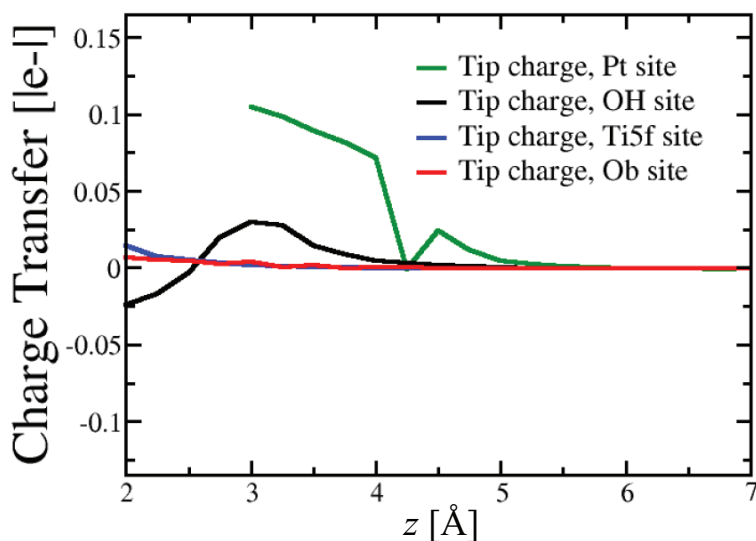


Fig. S5: Calculated electron transfer between a protrusion model tip and Pt/TiO₂ as a function of tip-sample distance. Bader charge analysis was used to estimate charge transfer in the simulations. An electron transfer between our model tip and Pt atom occurs for $z < 5.5$ Å, and that between tip and OH occurs for $z < 4.5$ Å.

The appearance of the ring-like structures over Pt atom positions in the LCPD map

The appearance of Pt atom positions as dark patches surrounded by darker rings in the LCPD map of Fig. 2(b) of the main manuscript can be explained by a relatively stronger force on top of the Pt atom position compared to the edges. As the tip scans across the sample surface, it senses the stronger attractive force just above the top of Pt atom position, as compared to the edges. To maintain a constant Δf , the tip has to retract from the top of Pt atom position. Consequently, the LCPD signal over the top ridge of the Pt atom shifts to higher values. Thus, the LCPD contrast over Pt atom positions appears as ring-like structure.

LCPD map of individual K atoms adsorbed on h -TiO₂(110) surface

In addition to the LCPD map acquired with a protrusion mode tip for the K adsorbed h -TiO₂(110) surface (see Fig. 2(d) in main manuscript), we here provide additional data sets acquired with a neutral mode tip. We also include the distance dependence of the LCPD shift over K atoms deposited on h -TiO₂ surface. The appearances of the individual K atoms in the NC-AFM images are shown in Fig. S6(a) and S6(b). The individual K atoms appear as protruding double-lobed structures (similar to coffee bean shape) over the two neighboring O_{br} rows in the NC-AFM topography (Fig. S6(a)) and Δf images (Fig. S6(b)). The most probable K sites are found to locate near O_{br} and between O_{br} and Ti_{5f} atomic rows.² By considering K mobility at RT and its interaction with the AFM tip, it is highly likely that the K atoms can jump over a Ti_{5f} atomic row, thus resulting in two-lobed structural appearances in the NC-AFM topography images.

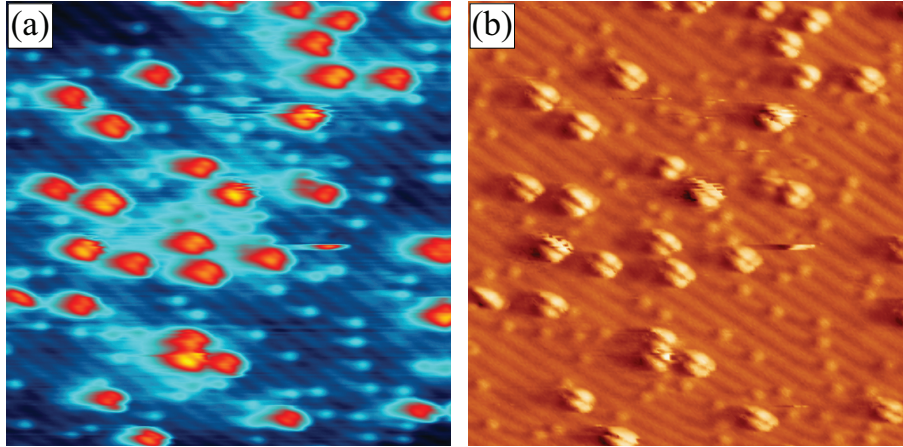


Fig. S6: (a) NC-AFM topography ($15 \times 15 \text{ nm}^2$) and (b) Δf images of the K adsorbed hydroxylated TiO₂(110) surface, acquired with a protrusion mode tip at room temperature. The bright protrusions with two lobe structures (i.e., coffee bean shape) indicate the K atoms. Acquisition parameters: $f_0 = 167.105 \text{ kHz}$, $A = 12.6 \text{ nm}$, $\Delta f = -2.7 \text{ Hz}$.

In Fig. S7(a) and (b), we show the NC-AFM topography and simultaneously measured KPFM images of the K adsorbed h -TiO₂ surface acquired with a neutral mode tip. A negative shift of LCPD signal appears over the K atom positions relative to the mean TiO₂ signal, which is an

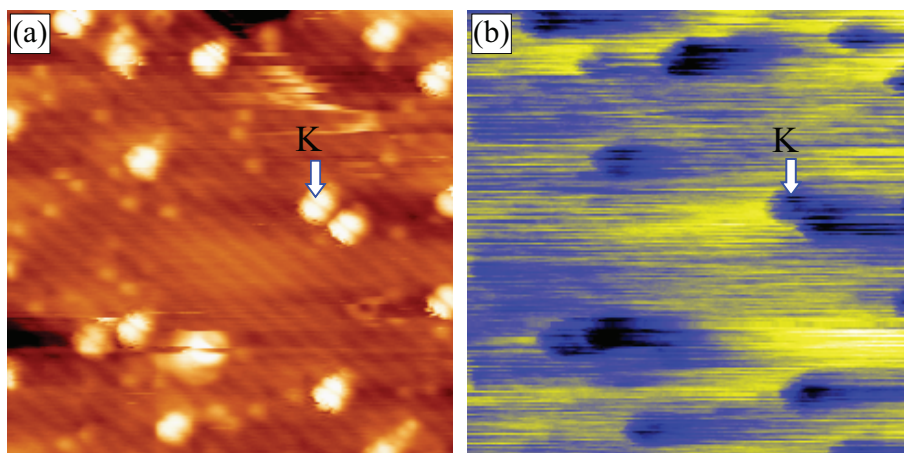


Fig. S7: (a) ($15 \times 14.25 \text{ nm}^2$) NC-AFM topography and (b) simultaneously obtained KPFM images of the K adsorbed hydroxylated $\text{TiO}_2(110)$ surface, acquired with a neutral mode tip at room temperature. The brighter features with coffee bean shape indicate the K atoms. The contrast above K atoms in the LCPD map is shifted to lower LCPD values compared to the substrate. Acquisition parameters: $f_0 = 165.311 \text{ kHz}$, $A = 13.4 \text{ nm}$, $\Delta f = -2.12 \text{ Hz}$. KPFM parameters: $U_{ac} = 0.5 \text{ V}$, $f_{ac} = 500 \text{ Hz}$.

indication of the fact that the K atom donates electrons to the substrate. Due to its low ionization potential, it is energetically favorable to transfer electron from K to the supporting substrate.³ It is worth noting that the neutral mode tip LCPD image shown in Fig. S7(b) shows qualitatively the same contrast as the protrusion mode tip LCPD image in Fig. 2(d) of the main manuscript, which confirms that the qualitative LCPD contrast is independent of tip states.

Fig. S8 displays the distance-dependent LCPD variation acquired with a protrusion mode tip over the K and OH atomic sites, i.e., two brightest atomic sites. We found that the distance dependence of the LCPD above the K and OH sites exhibits identical behavior as in the case of Pt atoms on $h\text{-TiO}_2$ surface. The LCPD drop over OH is relatively larger as compared with the one in Fig. 3(b) of the main manuscript. This might be related with the difference in details of the tip structure. While the observed image contrast clearly indicates the protrusion type tip-structure, a slight difference in the detail of tip-apex atomic structure can lead to an enhanced contrast in the LCPD map. Since the charge state of individual K atoms adsorbed on TiO_2 has been well-determined from different spectroscopic methods,^{4,5} the results presented here show a strong evidence that Pt and H atoms have identical charge state as K atoms, and suggest a charge transfer from Pt atom

to the substrate. These findings furthermore corroborate the generality of our results for other electropositive adsorbates on TiO_2 surfaces.

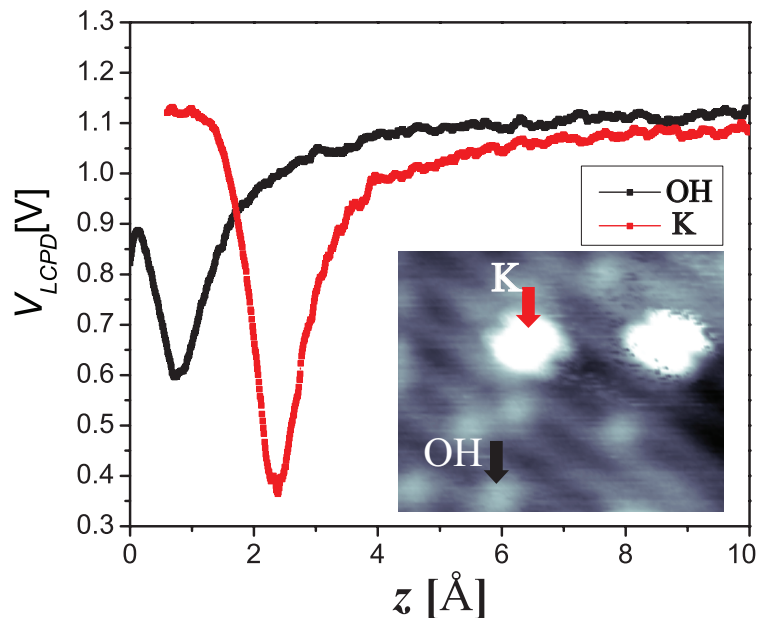


Fig. S8: Distance dependence of the LCPD above the K and OH atomic sites acquired using an active KPFM feedback to nullify existing electrostatic forces at each particular distance. Inset: NC-AFM image ($4.25 \times 3.5 \text{ nm}^2$) showing the individual K atom over which the spectroscopic measurements were performed. Acquisition parameters: $f_0 = 167.508 \text{ kHz}$, $\Delta f = -3.36 \text{ Hz}$. KPFM parameters: $U_{ac} = 0.5 \text{ V}$, $f_{ac} = 500 \text{ Hz}$.

References

- (1) Fernández-Torre, D.; Yurtsever, A.; Onoda, J.; Abe, M.; Morita, S.; Sugimoto, Y.; Pérez, R. *Phys. Rev. B* **2015**, *91*, 075401.
- (2) Yurtsever, A.; Sugimoto, Y.; Abe, M.; Matsunaga, K.; Tanaka, I.; Morita, S. *Phys. Rev. B* **2011**, *84*, 085413.
- (3) Pacchioni, G. *Phys.Chem.Chem.Phys.* **2013**, *15*, 1737–1757.
- (4) Heise, R.; Courths, R. *Surf. Sci.* **1995**, *331*, 1460–1466.
- (5) Prabhakaran, K.; Purdie, D.; Casanova, R.; Murny, C. A.; Hardman, P. J.; Wincott, P. L.; Thornton, G. *Phys. Rev. B* **1992**, *45*, 6969–6972.